Advances in engineering of high contrast CARS imaging endoscopes

Pascal Deladurantaye,[1,*] Alex Paquet,[1] Claude Paré,[1] Huimin Zheng,[1] Michel Doucet,[1] David Gay,[1] Michel Poirier,[1] Jean-François Cormier,[1] Ozzy Mermut,[1] Brian C. Wilson,[2,4] and Eric J. Seibel[3]

[1]INO, 2740, rue Einstein, Québec, G1P 4S4, Canada
[2]Princess Margaret Cancer Centre/university Health Network, and University of Toronto, Ontario, Canada
[3]University of Washington, Department of Mechanical Engineering, Seattle, Washington 98195, USA
[4]wilson@uhnres.utoronto.ca
**pascal.deladurantaye@ino.ca*

Abstract: The translation of CARS imaging towards real time, high resolution, chemically selective endoscopic tissue imaging applications is limited by a lack of sensitivity in CARS scanning probes sufficiently small for incorporation into endoscopes. We have developed here a custom double clad fiber (DCF)-based CARS probe which is designed to suppress the contaminant Four-Wave-Mixing (FWM) background generated within the fiber and integrated it into a fiber based scanning probe head of a few millimeters in diameter. The DCF includes a large mode area (LMA) core as a first means of reducing FWM generation by ~3 dB compared to commercially available, step-index single mode fibers. A micro-fabricated miniature optical filter (MOF) was grown on the distal end of the DCF to block the remaining FWM background from reaching the sample. The resulting probe was used to demonstrate high contrast images of polystyrene beads in the forward-CARS configuration with > 10 dB suppression of the FWM background. In epi-CARS geometry, images exhibited lower contrast due to the leakage of MOF-reflected FWM from the fiber core. Improvements concepts for the fiber probe are proposed for high contrast epi-CARS imaging to enable endoscopic implementation in clinical tissue assessment contexts, particularly in the early detection of endoluminal cancers and in tumor margin assessment.

OCIS codes: (060.2280) Fiber design and fabrication; (190.4380) Nonlinear optics, four-wave mixing; (300.6230) Spectroscopy, coherent anti-Stokes Raman scattering; (180.4315) Nonlinear microscopy.

References and links

1. R. Galli, V. Sablinskas, D. Dasevicius, A. Laurinavicius, F. Jankevicius, E. Koch, and G. Steiner, "Non-linear optical microscopy of kidney tumours," J. Biophoton. **7**(1-2), 23–27 (2014).
2. X. Xu, J. Cheng, M. J. Thrall, Z. Liu, X. Wang, and S. T. Wong, "Multimodal non-linear optical imaging for label-free differentiation of lung cancerous lesions from normal and desmoplastic tissues," Biomed. Opt. Express **4**(12), 2855–2868 (2013).
3. C. L. Evans and X. S. Xie, "Coherent anti-Stokes Raman scattering microscopy: chemical imaging for biology and medicine," Ann. Rev. Anal. Chem. **1**(1), 883–909 (2008).
4. C. L. Evans, X. Xu, S. Kesari, X. S. Xie, S. T. Wong, and G. S. Young, "Chemically-selective imaging of brain structures with CARS microscopy," Opt. Express **15**(19), 12076–12087 (2007).
5. C. M. Lee, C. J. Engelbrecht, T. D. Soper, F. Helmchen, and E. J. Seibel, "Scanning fiber endoscopy with highly flexible, 1 mm catheterscopes for wide-field, full-color imaging," J. Biophoton. **3**(5-6), 385–407 (2010).
6. E. Barhoum, R. Johnston, and E. Seibel, "Optical modeling of an ultrathin scanning fiber endoscope, a preliminary study of confocal versus non-confocal detection," Opt. Express **13**(19), 7548–7562 (2005).
7. B. G. Saar, R. S. Johnston, C. W. Freudiger, X. S. Xie, and E. J. Seibel, "Coherent Raman scanning fiber endoscopy," Opt. Lett. **36**(13), 2396–2398 (2011).
8. Z. Wang, L. Gao, P. Luo, Y. Yang, A. A. Hammoudi, K. K. Wong, and S. T. Wong, "Coherent anti-Stokes Raman scattering microscopy imaging with suppression of four-wave mixing in optical fibers," Opt. Express **19**(9), 7960–7970 (2011).

#217779 - $15.00 USD Received 25 Jul 2014; revised 4 Sep 2014; accepted 4 Sep 2014; published 7 Oct 2014

9. M. Balu, G. Liu, Z. Chen, B. J. Tromberg, and E. O. Potma, "Fiber delivered probe for efficient CARS imaging of tissues," Opt. Express **18**(3), 2380–2388 (2010).
10. C. S. Jun, B. Y. Kim, J. H. Park, J. Y. Lee, E. S. Lee, and D. I. Yeom, "Investigation of a four-wave mixing signal generated in fiber-delivered CARS microscopy," Appl. Opt. **49**(20), 3916–3921 (2010).
11. I. Veilleux, M. Doucet, P. Coté, S. Verreault, M. Fortin, P. Paradis, S. Leclair, R. S. Da Costa, B. C. Wilson, E. Seibel, O. Mermut, and J.-F. Cormier, "Design and modeling of a prototype fiber scanning CARS endoscope," Proc. SPIE **7558**, 75580D (2010).

1. Introduction

Coherent anti-Stokes Raman spectroscopy (CARS) is a label-free imaging modality that, by interrogating vibrational modes of bonds important in biological systems (e.g. CH_2 and CH_3 bonds present in large numbers in lipids and proteins as well as the O-P-O bonds in nucleic acid backbones), generates chemically selective contrast in tissue imaging. As a result, CARS has been used to differentiate normal from diseased tissue by, for example, highlighting the effects of transformation on protein and lipid density [1–4]. With the ability to identify diseased tissues in a real-time, label-free manner, CARS imaging promises to be a useful tool for the detection of tumor margins and other lesions in a surgical context. However, CARS systems are generally bulky, since they are usually based on free-space optics and employ bulky scan mirrors for image generation, and are thus unsuitable for use in endoscopic applications including use in surgical incisions or small lumens of organisms such as blood vessels. In order to apply CARS to minimally invasive endoscopic contexts, a miniaturized probe head must first be developed. Ideally, such a CARS probe head would be small enough to fit into the lumen of vessels and ducts in the human body, be highly flexible to follow their twists and turns and be capable of video rate acquisition to scan lesions in a clinically-practical time.

The recent development of scanning fiber endoscope (SFE) technology [5–7] has opened a promising route towards such a miniaturized probe head for CARS imaging. SFE scanners use a piezoelectric tube to actuate a cantilevered fiber tip, causing it to oscillate within the cross-sectional plane of the fiber. For wide-field reflectance and fluorescence imaging, the spiral shaped movement of the ultra-thin fiber tip allows scanning from a central point out to circles of >70° field of view, while providing images at scan rates >30 Hz. This technology has been applied to CARS to provide microscopic images of different structures in mouse skin [7]. However, although the scanning fiber probe provided good quality images, these images lacked chemical selectivity due to the presence of non-resonant background signal that contaminated the CARS signal. The probe design employed in that study using the same fiber core for both delivery of pump and Stokes beams and collection of CARS signal meant there was no straightforward means to reduce this background.

As reported by several other groups working on developing CARS based imaging for clinical applications, the non-resonant background is a significant problem that is difficult to address when fiber-optics are employed in the design of the probe [7–10]. Fiber dispersion makes the Stokes and pump pulses propagate at different speeds in the fiber, thus limiting their interaction length to a small section within the fiber. Experiments and modeling suggest that FWM generation is increased when the pump and Stokes pulses are synchronized either at the entrance or the exit of the fiber [10]. When the two pulses are synchronized at the middle of the fiber, for example, the FWM signal generated in the first half of the interaction is cancelled by the contribution from the second half [10], a typical situation for non-phase-matched nonlinear parametric processes. When the pulses coincide either at the entrance or exit of the fiber, however, such cancellation is compromised. This interpretation implies that a change of propagation medium (fiber core to air or vice versa, for example) can give rise to enhanced FWM signal. Although the magnitude of this FWM signal may be small compared to the pump and Stokes signals, for CARS applications the back-reflection of the small contaminant FWM signal by the sample itself becomes a significant issue, since the collected CARS signal is also very small. Since this FWM signal is composed of a wavelength identical to the measured Anti-Stokes emission, it can drown out the signal from the sample. While conventional forward-CARS systems can remove non-resonant background generated prior to

#217779 - $15.00 USD Received 25 Jul 2014; revised 4 Sep 2014; accepted 4 Sep 2014; published 7 Oct 2014

the sample by placing a simple long-pass filter before the scanning mirrors, this is not possible in epi-CARS based endoscopic systems. Thus mitigation strategies are required for reliable epi-CARS imaging.

One approach to markedly reduce the FWM signal is to use a separate fiber for CARS signal collection, allowing filtering of the output of the excitation fiber. In this scheme a dichroic mirror placed on the sample side of both fibers acts to remove the FWM signal from the delivery fiber output while redirecting the sample signal towards the capture fiber leading to the detector [9]. However, this requires free-space optics for scanning, leading to bulky probe heads (~cm diameter). A second approach having been proposed by Wang et al [8] relies on orthogonal polarizations of the pump and Stokes fields in a multimode polarization-maintaining fiber, minimizing the interaction between them and thus minimizing the FWM signal. In this scheme, the polarizations need to be realigned using a dual-wavelength waveplate upon exiting the fiber in order to generate the CARS signal at the sample. Unfortunately, because this setup requires a fixed waveplate orthogonal to the beam emitted by the fiber, a bulky free-space scanning system must be employed after the waveplate in order to obtain images. This setup is further limited to a single Raman band detection, as each pair of pump and Stokes beams requires its own custom waveplate, unlike optical filters which allow a range of combinations of wavelengths without altering the setup. Finally, the use of a multimode fiber leads both to lower resolution images due to a larger excitation spot size and lower CARS signal intensities due to the non-linear nature of CARS signal generation as compared to a single mode fiber based system.

In this paper we present an SFE-based scanning probe head containing a unique double-clad fiber (DCF) serving to both deliver the pump and Stokes pulses to the sample through the fiber core as well as provide a collection path for CARS signal in the inner (collection) cladding. This fiber is designed to reduce the level of FWM background which is generated within its single-mode core, as well as to ensure that bending losses are minimized so that it can be applied to challenging endoscopic applications. Furthermore, based on the inherent physical separation of the pump and Stokes delivery channel from the CARS signal collecting channel, we present a strategy to block the remaining FWM background from reaching the sample by using a microfabricated long-pass optical filter (MOF) scheme grown over the fiber core, leaving the cladding uncoated for CARS signal collection.

2. DCF development and characterization

2.1 Design and fabrication

A custom polarization-maintaining DCF was designed for use in CARS microendoscopy. The fiber core was designed to maximize the mode field area, since it has been previously demonstrated [10] that larger mode areas can mitigate the generation of FWM as well as other non-linear background signals. Although microstructured fibers represent an interesting option [9, 10], combining continual single-mode guiding and large mode areas, they were not considered here as the bending losses would become unacceptably high for endoscopic applications that may require fiber bending radii as small as 2 cm.

In order to achieve mode areas significantly larger than available from standard step index fibers, the design was based on a larger core with a lower numerical aperture, while preserving single-mode guiding. To reduce bending losses, a trench (negative refractive index depression) was introduced at some distance from the central axis. The trench parameters (depth and width) were optimized to minimize the LP_{01} bending losses at the Stokes wavelength (here, 1064 nm) at a 2-cm bending radius [Fig. 1(a)] while maximizing LP_{11} confinement losses at 816 nm (pump) to preserve effective single-mode guiding at this lower wavelength [Fig. 1(b)]. These tradeoffs led to the theoretical working design depicted in Fig. 1(c). This design should yield effective mode areas of 50 μm^2 at 816 nm and 80 μm^2 at 1064nm, which compare favourably against commercial off-the-shelf polarization-maintaining fibers that typically provide effective mode areas of around 20 and 40 μm^2, respectively, at these wavelengths. Thus, by reducing the intensity of the light in the core

#217779 - $15.00 USD Received 25 Jul 2014; revised 4 Sep 2014; accepted 4 Sep 2014; published 7 Oct 2014

compared to commercial fibers (e.g. PM780-HP, Nufern, East Granby, CT), a theoretical reduction of ~10 dB in FWM power can be roughly estimated, based on the intensity dependence of the FWM process: $I_{FWM} \propto I_{pump}^2 I_{Stokes}$. A more accurate estimate would imply a detailed modeling of the temporal dynamics involved in the FWM interaction, including phase-mismatch and pulse walk-off effects (both related to fiber dispersion), as well as other nonlinear effects such as self- and cross-phase modulation effects that affect the phase mismatch.

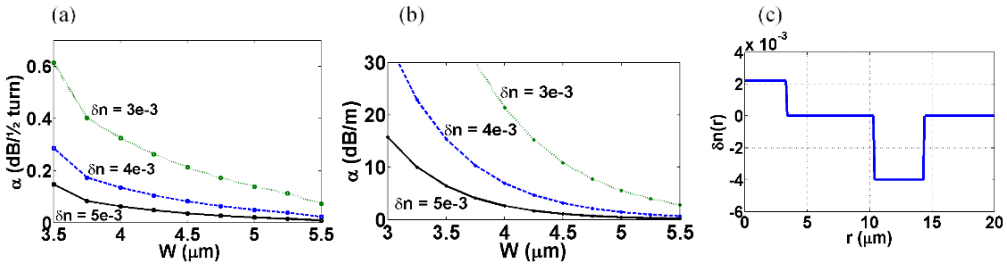

Fig. 1. Numerical evaluation of the influence of *W*, the trench width, and *δn*, the trench depth, on (a) bending losses per ½ turn at Stokes wavelength of 1064 nm for a 2-cm bending radius; (b) LP_{11} confinement losses at the pump wavelength of 816 nm. (c) Target index profile, designed to keep the bending losses at ~0.1 dB per ½ turn (2 cm bending radius) with mode field areas of 50 μm^2 at 816 nm and 80 μm^2 at 1064nm.

Surrounding the trench, the inner collection cladding was designed to efficiently collect the CARS signal from the sample and direct it back towards the detection chain on the proximal end of the fiber. Polarization holding is ensured by the stress-induced birefringence caused by the stress-applying parts (SAPs). The latter had to be slightly smaller and farther from the fiber axis than in typical polarization-maintaining fibers due to the presence of the trench, leading to a small sacrifice in fiber birefringence. Finally, fluorinated glass was chosen for the material of the outer cladding in order to maintain optimal optical and mechanical resonant properties of the fiber for SFE scanning.

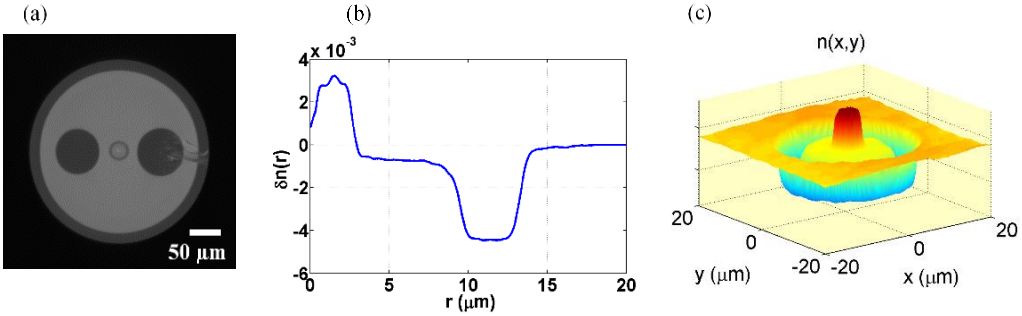

Fig. 2. (a) Picture of the fiber facet, (b) Relative radial refractive index profile of the INO-1006A11 DCF core, (c) 3D plot of the refractive index profile.

The designed DCF was fabricated using modified chemical vapour deposition (MCVD) technology and standard glass manipulation techniques. To achieve the targeted core index profile, germanium and fluorine were used as dopants. The fluorinated glass tube completed the preform assembly, which was drilled afterwards for the insertion of two boron-doped silica SAPs. The preform was then drawn to produce a DCF (INO1006A11) having a diameter of 245 ± 2 μm [Fig. 2(a)].

#217779 - $15.00 USD Received 25 Jul 2014; revised 4 Sep 2014; accepted 4 Sep 2014; published 7 Oct 2014

2.2 Characterization of index profile and FWM reduction

The measured index profile [Fig. 2(b)] shows a small departure from the targeted profile, with the largest divergence occurring mostly in the region between the core and the trench. This disparity gives rise to more confined fundamental modes that, in turn, lower the predicted reduction in FWM generation from 10 dB to about 4 dB in comparison to the PM780-HP. To test this prediction, comparative FWM level measurements were carried out with the INO-1006A11DCF and PM780-HP fiber segments (length ~2 m), using the setup depicted in Fig. 3(a).

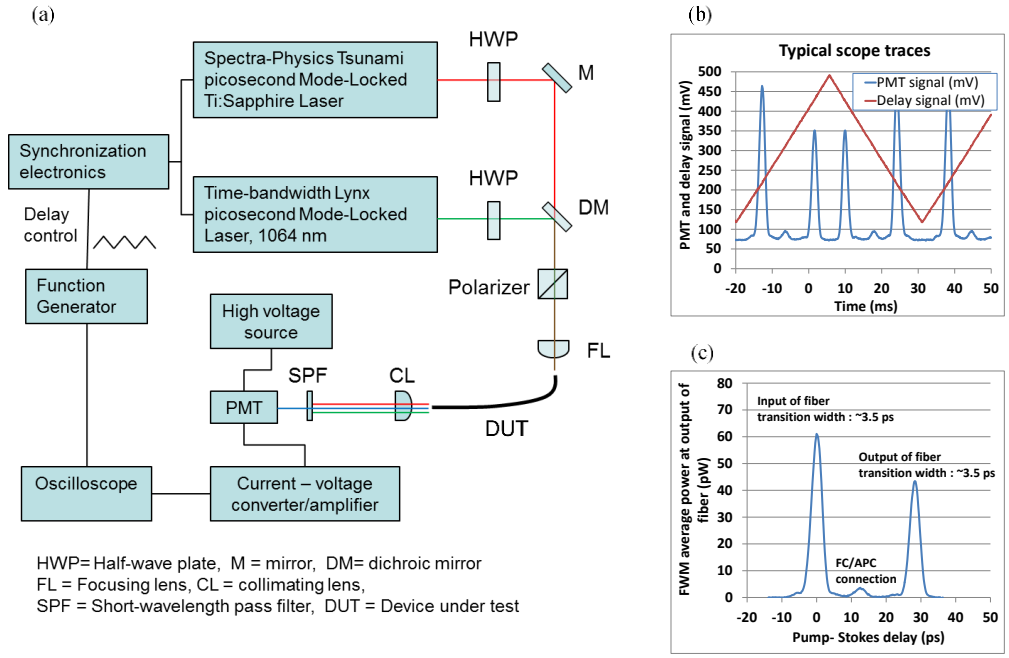

Fig. 3. (a) Block diagram of the CARS setup employed to characterize the contaminant FWM signal, A Spectra Physics Tsunami laser tuned to 816 nm was employed as the pump source and a Time-Bandwidth Lynx laser delivering 1064 nm acted as the Stokes source. The synchronization delay between the picosecond laser sources was modulated using a low frequency (~20 Hz) triangular wave. The emission of the pump and Stokes sources was coupled using a dichroic mirror and, after passing through a Glan–Thompson polarizer, was focused into the fiber core of the fiber under test, with the polarization aligned parallel to either the slow of the fast axis of the fiber. The fiber emission was filtered with a short pass filter to remove pump and Stokes wavelengths, allowing anti-Stokes/FWM wavelengths to be detected by a photomultiplier tube (PMT). The PMT signal was then amplified and converted from current to voltage for display on the oscilloscope along with the function generator output. (b) Typical oscilloscope traces showing FWM peaks detected at delays corresponding to air-glass interfaces, (c) graph showing typical actual FWM power vs actual delay.

The average power level coupled in the core of the fibers under test was ~60 mW for the pump wave and ~40 mW for the Stokes wave. For the PM780-HP fiber, these values were measured with a power meter placed directly at the output of the fiber. For the DCF, an image of the fiber distal facet was created and centered on a pinhole placed in front of the detector to measure only that part of the emission coming from the single mode core, while blocking the residual uncoupled light emitted from the inner collection cladding. A photomultiplier tube was used to detect the FWM signal as a function of the synchronization delay between the lasers, corresponding to pulse interactions at different locations along the fiber [typical oscilloscope trace shown in Fig. 3(b)]. The detection chain transfer function was characterized in order to extract actual FWM power values (in pW) emitted by the fiber [Fig. 3(c)]. Sharp FWM peaks were detected at delays corresponding to air-glass interfaces, a result

#217779 - $15.00 USD Received 25 Jul 2014; revised 4 Sep 2014; accepted 4 Sep 2014; published 7 Oct 2014

similar to that reported in [10]. To benchmark the FWM generation in the DCF, the FWM peak power was measured for the peak corresponding to the fiber distal air-glass interface, for both the 1006A11 DCF and the PM780-HP fiber. Using this method, a reduction of (3 ± 1) dB of the FWM noise was observed with the 1006A11 over three measurements, compared to the reference fiber, which is in good agreement with the 4 dB value estimated from the mode field areas.

2.3 Characterization of beam quality

In optical fibers, the presence of higher-order modes can deteriorate the beam quality (increase of the beam propagation factor, M^2) and so decrease the ability to achieve the tight focus needed for high-resolution imaging. Hence, it is important to assure that the DCF central core will maintain robust single-mode operation at both the Stokes and pump wavelengths. M^2 measurements were carried out at 816 nm (near the bottom of the design wavelength range) using a Spiricon M^2-200s beam analysis instrument, examining a 2m long DCF segment, as depicted in Fig. 4(a). To ensure the robustness of the single-mode operation, the M^2 value was additionally measured while purposely detuning the alignment of a single transverse mode beam launched into the optical fiber so as to induce a 50% reduction of the coupling efficiency obtained with optimal alignment. In this configuration, the excitation of higher-order modes is favored, especially close to the theoretical cut-off wavelength for single-mode operation (lower end of the design wavelength range). An M^2 value of 1.05 ± 0.01 was obtained for both launching conditions, which is close to the expected value for the fundamental LP_{01} mode (M^2 ≈1.03, mode calculated from the measured index profile), indicating single-mode content. Further testing showed 75% reduction of the coupling efficiency was required before an observable increase of the M^2 (e.g. M^2 ~1.1) occurred.

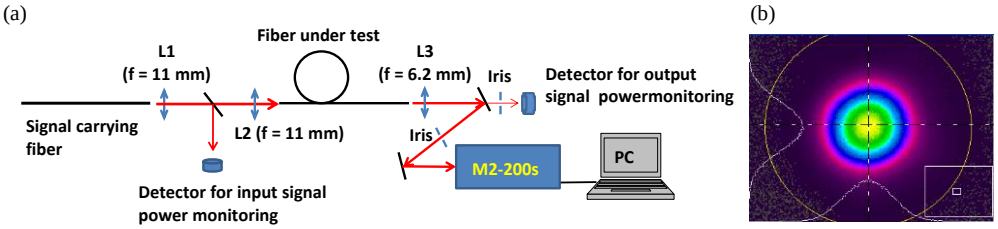

Fig. 4. (a) Test setup for measurement of beam propagation factor. (b) Typical near field output beam profile obtained while purposely detuning the alignment of a single transverse mode beam launched in the optical fiber so as to induce a 50% reduction of the coupling efficiency from optimal alignment. M^2 = 1.05 ± 0.01.

2.4 Characterization of bending losses

Bending losses for the DCF core were assessed by measuring the loss induced by coiling the fiber 8 turns around a 39 mm-diameter post. Since bending losses are expected to be more problematic for longer wavelengths, they were determined using the 1064 nm pump beam. This was < 1.2 dB, corresponding to < 0.08 dB (or ≈2% loss) per ½ turn, which is close to the targeted value of ~0.1 dB. This compares advantageously to the result obtained using the same method with the Nufern PM780-HP fiber (0.14 dB or ≈4% loss per ½ turn). The bending losses of the multimode collecting cladding were also assessed at 660 nm using the same method, yielding < 0.10 dB (or ≈2.3% loss) per ½ turn. These values are quite reasonable for the intended endoscopy applications such as in the gastrointestinal tract and gently curving branches of the pulmonary and cardiovascular systems.

2.5 Polarization-maintaining performances

As previously mentioned, due to design considerations the fiber birefringence ($B = 2 \times 10^{-4}$) is not as high in the 1006A11 DCF as it is for commercial polarization-maintaining fibers like

#217779 - $15.00 USD Received 25 Jul 2014; revised 4 Sep 2014; accepted 4 Sep 2014; published 7 Oct 2014

the PM780-HP ($B = 3.3 \times 10^{-4}$). A polarization extinction ratio (PER) of 18 dB was measured at 816 nm for a 2 m-long piece of 1006A11 fiber, using a polarizing beam splitter at the output of the fiber. Compared to a measured PER of 21 dB for the PM780-HP fiber, the 1006A11 fiber shows a slightly reduced ability to maintain polarization. In principle, this should not affect the CARS generation efficiency by more than a few percent for given pump and Stokes power levels.

3. Integration with CARS imaging scanning fiber probe

To achieve the mechanical scanning functionality needed for endoscopic CARS image generation, the DCF was integrated into an SFE-based scanning probe head, as shown in Fig. 5. A ceramic piezoelectric actuator was used to drive the DCF tip in an expanding spiral configuration by actuating the fiber at its mechanical resonance in orthogonal directions 90° out of phase in its cross-sectional plane, as previously described [5]. The actuator was driven at low voltage with customized algorithms/software by a hollow piezoelectric transducer consisting of a metal coated poled raw ceramic tubes (type 5a, Morgan Technical Ceramics Sales, Fairfield, N.J), machined to the proper length with metal quadrant electrodes formed by removing portions of the metal coating.

Calibration of the scanner head to achieve efficient spiral scanning and breaking [5] was performed using a custom calibration module. An outer metal sheath with a 3mm diameter served to protect the fiber end. Although the eventual goal is to integrate a small diameter objective lens into this sheath [11], for the present purpose off-the-shelf microscope objectives (Mitutoyo NIR 5X) were mounted in front of the scanning probe head instead. The determined imaging speed at maximum scan rate for the integrated probe was just under 20 Hz.

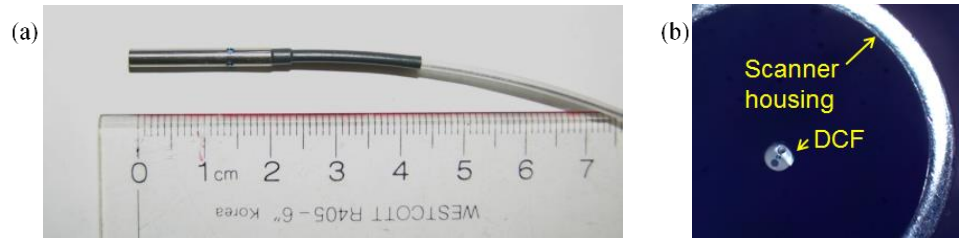

Fig. 5. Images of the developed SFE probe head. (a) Side view. (b) Front view (DCF diameter is 245 μm).

The setup shown in Fig. 3(a) was modified to conduct an initial imaging test on 6μm polystyrene (PS) beads in air using epi-CARS configuration as shown in Fig. 6(a). The beads were deposited on a mirror to emulate the worst-case FWM background reflection. The images demonstrated very low contrast [Fig. 6(b)] with a ratio of ~0.7 [Fig. 6(c)] between the mirror-reflected FWM signal and the PS-bead signal (combination of reflected FWM background and CARS signal), yielding a corresponding sample CARS/FWM ratio of only ~0.4.

#217779 - $15.00 USD Received 25 Jul 2014; revised 4 Sep 2014; accepted 4 Sep 2014; published 7 Oct 2014

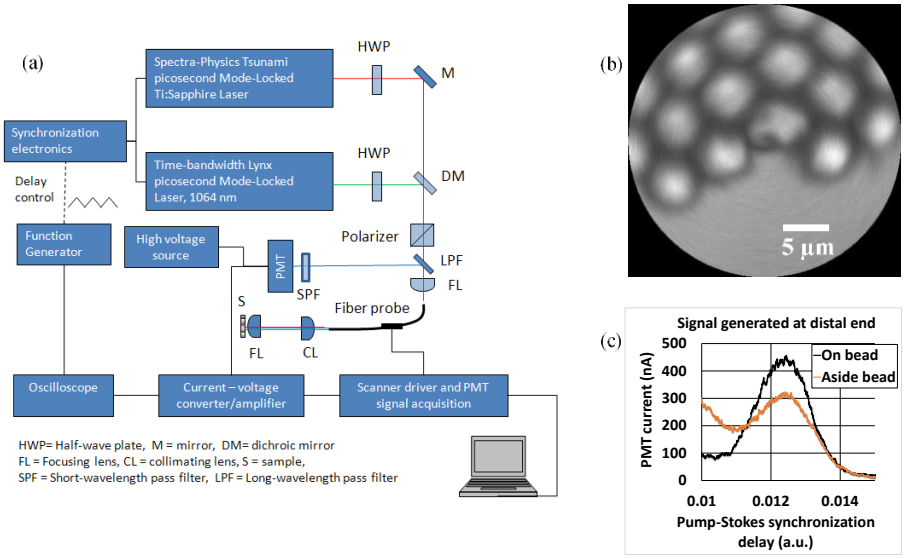

Fig. 6. (a) Epi-CARS setup employing a Spectra-Physics Tsunami laser tuned to 816 nm at 44 mW and a Time-Bandwidth Lynx laser tuned to 1064 nm at 22 mW, for excitation of Raman transitions around 2850 cm^{-1}. A collimating lens and focusing lens (two Mitutoyo NIR 5X objectives) were used to deliver the pump and Stokes beams to the sample. Anti-Stokes light from the sample ($\lambda_{Anti\text{-}Stokes}$ = 662 nm) was collected and directed back along the same path to the fiber, where it was collected by the core and surrounding inner cladding. The light was then directed to a PMT using a long-pass dichroic mirror and short-pass filtered to remove the pump and Stokes radiation. (b) Epi-CARS image of (6µm) polystyrene beads deposited on a mirror at ~2850 cm^{-1} using the DCF-based SFE. (c) Signal detected at 662 while on and aside beads.

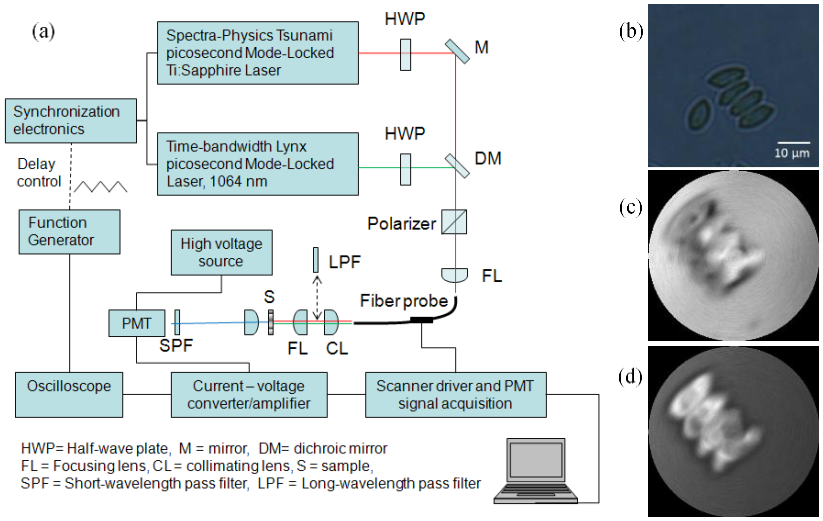

Fig. 7. (a) Forward CARS setup. The pump and Stokes beams were delivered to the sample as for the epi-CARS setup except that a long-pass filter was employed between the focusing and collimating lens for some images. Anti-stokes light was collected in the forward direction by an objective lens and, after removal of pump and Stokes radiation with a short-pass filter, directed onto a PMT. Images of micro-algae obtained by optical transmission microscopy (b) and F-CARS without (c) and with (d) filtering of the FWM contaminating signal generated in the probe fiber. Different regions of the same sample were used for CARS vs optical microscopy.

#217779 - $15.00 USD Received 25 Jul 2014; revised 4 Sep 2014; accepted 4 Sep 2014; published 7 Oct 2014

To ensure that the lack of contrast arose due to significant FWM contaminant signal, further imaging was performed in a forward CARS configuration [Fig. 7(a)], in which a long pass filter was used to block the FWM signal generated in the fiber. Using this setup to image micro-algae, as a biological demonstrator example, a large improvement in the signal to background was observed [Figs. 7(c) and 7(d)]. Hence, it is clear further reduction of the level of FWM in the signal is required generate high-contrast, chemically-selective images using the scanning probe in the epi-CARS configuration, which is the purpose of the MOF scheme presented in the next section.

4. Microfabricated optical filter (MOF) development and characterization

As a strategy to eliminate the FWM signal generated in the optical fiber, a microfabricated optical filter (MOF) was designed which could be grown on the end of the DCF to cover only the fiber core, as schematically represented in Fig. 8(a). This would act as a long-wave edge-pass filter to reflect short wavelength (e.g. 662 nm) FWM light but transmit the pump and Stokes beams. Simulations were performed to determine the optimal size of the filter to maximally block the FWM signal from the core while minimizing the CARS signal blocked from entering the collection cladding. The collection efficiency of the DCF collection cladding in the presence of different size MOFs were modelled using the same method and tissue optical parameters as previously reported [11]. It was determined that the efficiency of collection would be significantly reduced at MOF diameters larger than 40µm [Fig. 8(d)]. On the other hand, MOF <25µm would result in unwanted diffraction effects on the emitted (excitation) light.

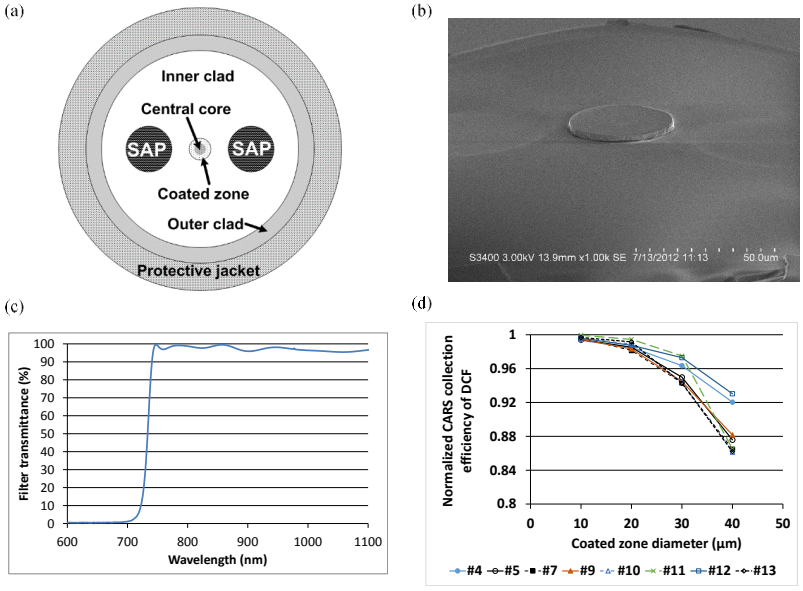

Fig. 8. (a) Schematic of the DCF with MOF. (b) SEM images of the DCF tip with MOF. (c) Measured MOF spectral transmittance. (d) Calculated DCF CARS collection efficiency as a function of MOF size for a variety of modeled samples (identified by #4,5,7,9,10,11,12,13, the corresponding tissue parameters can be found in Table 4 of *Veilleux et al., Proceedings of the SPIE, Volume 7558, article id. 75580D, 2010*).

For experimental testing, the MOF was grown on the distal tip of the DCF by photolithography. Briefly, after cleaving the fiber with a CO_2 laser, a layer of photoresist was applied to the fiber tip by dipping. The photoresist was then activated with a UV source through a pinhole to generate an exposed circle with a diameter of 37 µm centered on the fiber core. The exposed resist was chemically removed and dielectric layers, consisting of a stack of 29 alternating layers of ZrO_2 and SiO_2 of 2.67 µm total thickness, were deposited on

#217779 - $15.00 USD Received 25 Jul 2014; revised 4 Sep 2014; accepted 4 Sep 2014; published 7 Oct 2014

the masked fiber facet. The unexposed resist was then chemically removed, leaving the MOF formed on the fiber core [Fig. 8(b)]. A typical spectral transmittance curve of is shown in Fig. 8(c), showing > 95% transmittance between 750 and 1100 nm, thereby ensuring minimal losses for the CARS pump and Stokes waves. Thus, e.g. for exciting the symmetric CH_2 stretching vibration at 2845 cm^{-1}, the very low transmittance of this coating at 662 nm (< 1%) should attenuate the contaminant FWM background by more than two orders of magnitude. Several such fiber devices were fabricated and showed repeatable performance.

In order to ascertain the effectiveness of the MOF on reducing the level of FWM background for the DCF, epi-CARS imaging and FWM measurements were performed on DCFs with or without MOFs. The FWM background was first measured with a DCF lacking MOF, in the presence and absence of a mirror at the sample plane. A tenfold increase in the FWM signal was measured in the presence of the mirror. Assuming that 4% of the FWM is reflected back at the DCF distal end (Fresnel reflection) and taking into account insertion losses into the objective lens, this increase in FWM signal is within the expected range. Using the same setup and pump and probe power settings, the probe terminated by a MOF was also tested. Typical PMT current values lying between 500 nA and 1 µA were measured, which is 10-20 times higher than the values obtained without the MOF and with no mirror at the sample position. These are also slightly higher than the values without the MOF but with the mirror at the sample plane. This indicates that the MOF does not inhibit FWM generation but instead reflects the FWM background towards the proximal end of the probe. Thus, a spatial filter is required to selectively block the FWM background that is returned through the fiber core, while minimally affecting the CARS signal collected through the outer collection cladding in order to achieve high-contrast imaging.

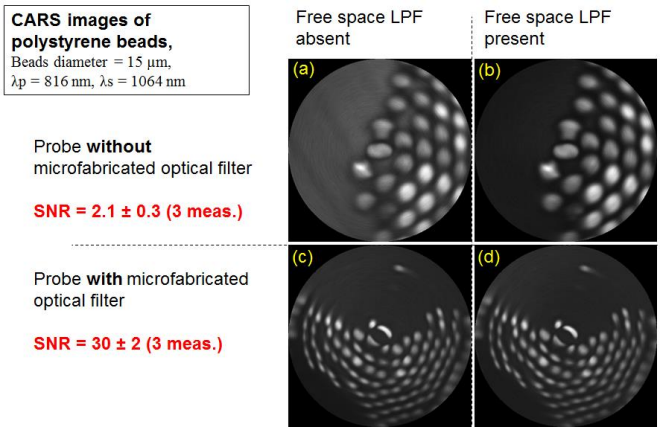

Fig. 9. CARS images of 15µm polystyrene beads taken using the forward-CARS setup with (a) DCF without MOF and no free-space LPF, (b) DCF without MOF with free-space LPF, (c) DCF with MOF without free-space LPF and (d) DCF with MOF and free space LPF.

To further examine the ability of the MOF to block FWM, CARS imaging of polystyrene beads was conducted using DCFs with and without MOFs in the forward-CARS setup [Fig. 7(a)]. This setup allows insertion of a long-pass filter between the DCF probe distal tip and the sample to block the shorter wavelength contaminant signal so it does not reach the sample. The images in Fig. 9 show that insertion of the LPF significantly improved the contrast for the non-MOF probe but there was no noticeable improvements for the MOF probe. Although qualitative, this result suggests that the MOF does remove the FWM component efficiently. To assess this quantitatively, PMT signals were measured for both types of probe under the following conditions: 1) with LPF and sample in place (*SF*), 2) LPF present without sample (*NSF*), and 3) no sample and no LPF (*NSNF*). A signal-to-noise ratio was defined for a given probe as $SNR = (SF-NSF)/(NSNF-NSF)$. This represents a figure of merit of a probe to generate contrasted CARS images, as its value is principally determined

#217779 - $15.00 USD Received 25 Jul 2014; revised 4 Sep 2014; accepted 4 Sep 2014; published 7 Oct 2014

by the ratio of the CARS signal measured with a reference sample (*SF*) to the FWM noise emitted by the probe (NSNF), taking into account the background detection (*NSF*) due to factors such as the finite extinction of the SPF, the electronic detection noise and the signal originating from residual ambient light. For the DC- based probe without MOF, an SNR of 2.1 was calculated over 3 readings, while the probe with MOF had an SNR of 30 over 3 measurements. This represents an 11.5 dB improvement [Fig. 9], showing that the MOF is effective at blocking the FWM signal from reaching the sample.

To characterize the FWM-blocking performance of the MOF-terminated DCF in epi-CARS configuration, the setup [Fig. 6(a)] was modified by adding a lens between the long-pass dichroic mirror and the short-pass filter directly in front of the PMT, creating a conjugate plane of the proximal end of the DCF fiber. At this plane a spatial filter consisting of a round 60μm diameter metallic disk deposited on a glass substrate could be positioned to block the light from the DCF core. FWM measurements were then carried out without sample present at the sample plane. Although, in the absence of the spatial filter, a significant level of contaminant signal was observed returning from the fiber core as expected, only a 30% reduction in contaminant signal was observed in the presence of the spatial filter compared to the expected 15-fold decrease required to match the results from the forward-CARS experiment. Since the effectiveness of the spatial filter was tested using a pure single-mode fiber-coupled laser and found to have an extinction ratio of 32:1, these results seem to indicate that the FWM signal is not fully confined to the fiber core. In order to confirm this, the PMT was replaced by a camera to image the proximal end of the DCF. Although these images showed a significant level of FWM concentrated in the fiber core, a significant amount of FWM was detected in the collection cladding as well [Fig. 10].

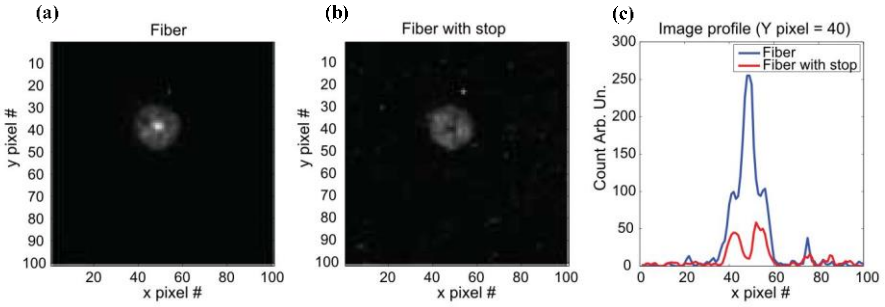

Fig. 10. CCD images and linear intensity profiles of FWM emission at proximal end of INO DCF in epi-CARS setup. (a) Image obtained without spatial filter in place, (b) Image with spatial filter in conjugate plane, (c) Intensity profile along a horizontal line coinciding with the center of the fiber tip image.

Since high contrast CARS images were obtained in the forward-CARS configuration using scanning probes with MOFs, it appears that the FWM background reflected by the MOF may not be totally coupled back in the central core. A possible origin of the presence of FWM in the collection cladding in the epi-CARS configuration could be linked with some residual angle that may exist between the fiber optical axis and the MOF surface normal due to fiber facet curvatures left by the CO_2 laser cleaving process [Fig. 11(a)]. Given the low numerical aperture (NA ~0.08) of the central core, part of the FWM noise could be reflected at angles too large to be captured by the core, escaping into the outer cladding which has higher NA (0.2). To support this theory, we numerically estimated the power recoupling efficiency of an LP_{01} guided mode at 663 nm (the single-mode cut-off for the 1006A11 DCF is ~600 nm) after its own reflection from a flat but misaligned perfect mirror. Figure 11(b) shows that minor deviations as small as 1° could lead to a ~60% recoupling efficiency, indicating that ~40% of the light could potentially escape to the cladding.

Further analysis also suggests that a core that is bi-modal (also guiding LP_{11} mode) at 663 nm while remaining single-mode at the pump and Stokes wavelengths would be much more

#217779 - $15.00 USD Received 25 Jul 2014; revised 4 Sep 2014; accepted 4 Sep 2014; published 7 Oct 2014

immune to MOF misalignment, since most of the LP_{01} reflection would remain trapped within the core because most of the ~40% power not coupled to LP_{01} would be in the LP_{11} mode. Additionally, although not detected, hypothetical defects causing scattering at the MOF-fiber interface could also generate angular components, leading to reflections of FWM signal not captured by the central core.

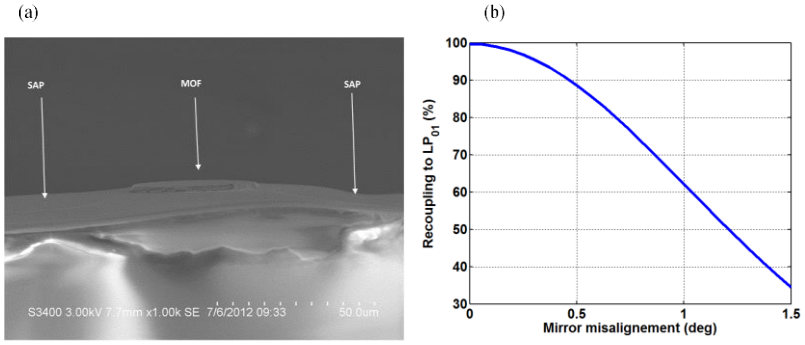

Fig. 11. (a) SEM image taken at a shallow angle showing curvatures of the fiber distal facet close to the MOF; (b) Estimated power recoupling into LP_{01} mode at 663 nm after back-reflection from a misaligned mirror.

5. Conclusions

A proof-of-concept SFE CARS probe based on a customized dual-clad fiber has been designed and demonstrated. This approach, combining illumination and collection in a single fiber and relying on miniature fiber scanner technology, enables CARS to be performed with small diameter probe heads suitable for endoscopy. Compared to the commercially available PM780-HP fiber, the developed LMA DCF design provides a 2-fold reduction in both the FWM generated in the fiber and the bending losses at coiling diameters required in endoscopy. Custom miniature optical filters, designed and grown on the distal end of these DCFs, block the FWM signal generated in the fiber from reaching the sample while having a minimal impact on CARS collection efficiency and no impact on the probe footprint. In epi-CARS configuration, however, these first devices suffer from insufficient confinement of the MOF-reflected FWM light into the single mode core, so that a portion of the FWM signal could enter directly into the collection cladding and contaminate the sample CARS signal. We hypothesize that the root causes of this crosstalk between the single-mode core and the second clad of the DCF is imperfect orientation of the MOF with respect to the DCF optical axis and/or scattering defects at the MOF-fiber interface. Nevertheless, imaging in the forward CARS configuration has shown that the MOF enables high-contrast chemically-selective imaging at quasi-video rate. Refinements of the fabrication of the DCF to match the idealized core index profile should provide a further intrinsic 10 dB reduction of the FWM. The fiber design could also be modified so as to make the core bi-modal at 663 nm (while remaining single-mode at the pump wavelength) in order to improve the confinement of the FWM to the central core in the MOF approach, and the fiber-cleaving procedure could be modified to ensure optimal orientation of the MOF with respect to the fiber axis. Such improvements will lead to a DCF-based system capable of performing CARS imaging in surgical contexts, with many applications, including label-free tumour identification.

Acknowledgments

Technical support was provided by Rich Johnston and Dave Melville from the Human photonics Lab, University of Washington, Seattle for the custom fiber scanner fabrication. The authors also want to thank Rob Brown, Benoît Fortin, Carl Larouche and Samir Ilias from INO, Quebec City, for their technical support. Funding was provided in part by NIH R21 EB012666 (Seibel).